Schnubel, D.; Huber, N.:

The influence of crack face contact on the prediction of fatigue crack propagation in residual stress fields

In: Engineering Fracture Mechanics (2011) Elsevier

DOI: 10.1016/j.engfracmech.2011.12.008

The influence of crack face contact on the prediction of fatigue crack propagation in residual stress fields

D. Schnubel*, N. Huber

Institute of Materials Research, Materials Mechanics,
Helmholtz-Zentrum Geesthacht, Max-Planck-Straße 1, 21502 Geesthacht, Germany

accepted for publication doi:10.1016/j.engfracmech.2011.12.008

Abstract

It is a common practise to predict fatigue crack propagation rates for specimens containing residual stresses using the weight function or finite element method. Due to combined applied load and internal residual stresses, the stress intensity factor K_{tot} at the crack tip is calculated and used to predict the resulting fatigue crack propagation rates in conjunction with empirical crack growth laws. The calculation of K_{tot} normally implies pure linear elastic behaviour and the validity of the superposition law. For cracks growing through areas of high compressive residual stresses and subsequent transition areas from compressive to tensile residual stresses, this assumption is not necessarily valid. In this case the definition of non-linear contact conditions on the crack faces becomes necessary to describe the problem in a physically sound way. The presented study discusses the resulting differences in the prediction results for the case of an aluminium C(T)100 specimen containing a residual stress pattern typically found after welding processes.

Keywords: Stress intensity factor, Residual stresses, Fatigue crack propagation, Fatigue crack growth, Damage tolerance

*Corresponding author. Tel: +49 4152 87-2637. URL: www.hzg.de
Email addresses: dirk.schnubel@hzg.de (D. Schnubel), norbert.huber@hzg.de (N. Huber)

Nomenclature

C	Material constant of the Walker equation
E	Young's modulus
$E_{\epsilon,\mathrm{norm}}$	Normalised stored strain energy
F_{max}	Maximum applied load of a load cycle
F_{min}	Minimum applied load of a load cycle
G_{tot}	Total energy release rate
K_{appl}	Stress intensity factor due to applied load
K_{res}	Stress intensity factor due to internal residual stresses
K_{tot}	Total stress intensity factor due to the combination of applied load and internal residual stresses
N	Number of load cycles
R_{tot}	Total stress intensity ratio
ΔK_{tot}	Total stress intensity factor range
Δa	Crack growth increment
$\mathrm{d}a/\mathrm{d}N$	Fatigue crack propagation rate
ν	Poisson's ratio
σ_{yy}	Stress component acting perpendicular to the crack growth direction
a	Crack length
m	Material constant of the Walker equation
n	Material constant of the Walker equation

1. Introduction

Due to significant advantages regarding production costs, weight reduction and corrosion resistance, the use of advanced joining technologies, such as laser beam welding or friction stir welding, in the manufacture of metallic aircraft structures is increasing [1, 2]. During welding, high residual stresses are induced in the structures [3, 4], influencing the fatigue crack propagation behaviour significantly [5, 6]. In the design of such structures, the methodology of damage tolerance is applied, which, as one central element, implies the possibility of an accurate prediction of the fatigue crack propagation. Consequently, there is an increasing interest in prediction methodologies that also consider the influence of the welding-induced residual stresses. As the presence of residual stresses directly influences the observed stress intensity at the crack tip during cyclic loading, the general methodology to perform such predictions is well accepted [5–17] and consists of the following steps:

1. Calculation of the stress intensity factor K_{tot} resulting from the combined applied load and residual stresses as a function of the crack length a.
2. Calculation of the corresponding total acting stress intensity factor range ΔK_{tot} and stress intensity factor ratio R_{tot}.
3. Prediction of the fatigue crack propagation rate $\mathrm{d}a/\mathrm{d}N$ using ΔK_{tot} and R_{tot} in empirical crack growth laws, such as the Walker equation.
4. Prediction of the crack length a as a function of the load cycles N by numerical integration of the fatigue crack propagation rate $\mathrm{d}a/\mathrm{d}N$.

However, for the calculation of K_{tot}, there are several different methods available, if only linear elastic material behaviour is considered. The two most popular ones are the analytical weight functions method (WFM) and the numerical finite element method (FEM). Both methods deliver similar results applied to the same problem, as demonstrated in [14] for the specific case of a crack growing in the residual tensile stress field of an aluminium alloy AA2024 weld.

The WFM has the advantage of delivering very fast predictions [7, 14, 17]. However, the knowledge of the weight functions corresponding to the used specimen geometry is mandatory for its use. The FEM can be applied directly to arbitrary geometries, and stress redistribution effects during crack growth are covered naturally without any additional effort [13, 18]. If linear elastic behaviour is assumed, for both WFM and FEM, the calculation of K_{tot} can be derived by using the superposition principle as given in Eq. (1). Thus, the stress intensity created by the combination of two or more loads can be obtained by adding the independently calculated contribution of any individual load [7].

$$K_{\mathrm{tot}} = K_{\mathrm{res}} + K_{\mathrm{appl}} \tag{1}$$

One calculation per crack length is then needed to find the stress intensity factor due to the residual stresses K_{res} in the absence of external loads via WFM or FEM. Because the stress intensity due to the applied load K_{appl} is often well known for standard geometries, e.g., in the form of handbook solutions, K_{tot} can

be calculated for arbitrary load cases in a fast way using Eq. (1). This approach is very elegant and delivers results at minimum calculation costs. Even if an overlap of the crack faces occurs in the calculation of K_{res}, the calculated K_{tot} using the superposition principle are still physically sound as long as the applied load is high enough that the crack faces are completely opened over the whole crack length under combined loading. However, for cracks located in high compressive residual stress fields, it is possible, that the crack faces in the calculations show an overlapping even under applied loading. A direct consequence is the possible appearance of negative K_{tot}.

The most simple and therefore commonly used approach to deal with negative K_{tot} is to set them to zero during the following calculation steps [6, 7, 10, 16], as described later. Unfortunately, this course of action does not lead to a physically sound description of the problem. As stated by Parker [7], superposition of stress intensity contributions may produce physically unacceptable answers in that case. Irving et al. [6] noted that following this approach leads towards predicting the experimentally measured fatigue crack growth rates, but the agreement is not ideal.

For both WFM and FEM, it is also possible to implement real contact corrections. While iteratively additional contact forces can be introduced to suppress overlapping in the WFM [7, 15], a hard contact condition can be defined in FEM to prevent the interference of the crack faces [15, 19]. In both cases, non-linearities are introduced that do not allow the application of the superposition principle. Hence, it becomes mandatory to extract K_{tot} directly from a model being simultaneously subjected to both the applied load and the residual stresses because, in this situation, the crack opening depends non-linearly on the applied load.

The work presented in this paper discusses the question of how large the resulting differences in the prediction results are, using the common approach of simply setting negative K_{tot} to zero and introducing a realistic contact correction. To do so, FEM is used with and without hard contact definition on the crack faces to predict the fatigue crack propagation rates for an aluminium C(T)100 specimen, on which an assumed (virtual) welding residual stress profile was mapped.

2. Modelling approach

2.1. Prototype residual stress profile

To imitate a longitudinal residual stress profile as it is typically observed after aluminium butt joint welding [3], an analytical prototype residual stress profile [14, 17, 20], as given in Eq. (2), was used with the selected parameters values $\sigma_0 = 150$ MPa, $c_0 = 10$ mm and $x_0 = 50$ mm. For reference calculations without residual stresses, the parameter σ_0 was set to 0 MPa. Figure 1 shows the corresponding curves with residual stresses ("RS") and without residual stresses ("No RS") .

$$\sigma_{\mathrm{yy}}(x) = \sigma_0 \left(1 - \left[\frac{x - x_0}{c_0}\right]^2\right) \exp\left(-\frac{1}{2}\left[\frac{x - x_0}{c_0}\right]^2\right) \tag{2}$$

In comparison with measured longitudinal stress profiles in real aluminium welds [3], the assumed stress peak amplitudes in tension and compression are in a realistic range, even though the shape of real stress profiles is more complex. The use of this simplified profile allows a comprehensive discussion of the impact of the simulation boundary conditions on the predicted crack propagation rates.

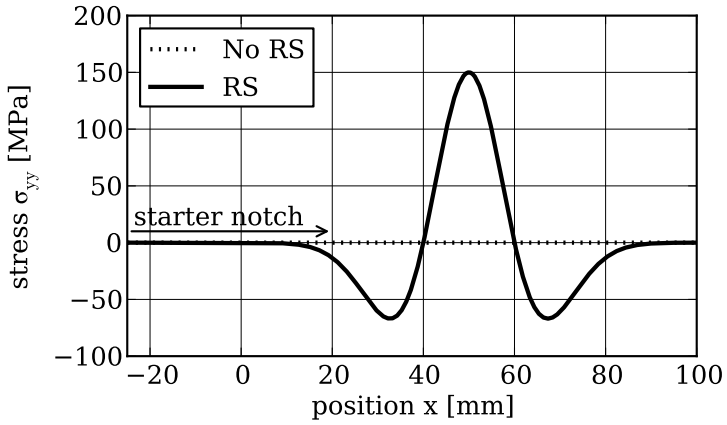

Figure 1: Model distribution of a longitudinal welding residual stress profile "RS" (Eq. (2)) and the reference case without residual stresses "No RS".

2.2. FE Model

A FE model representing a C(T)100 specimen that corresponds to the definitions in ASTM E647 [21], but with a thickness of only 5 mm, was built for use with the FE software Abaqus. To reduce the modelling effort, fixture holes and the starter notch were not explicitly modelled. The specimen was meshed with a constant element size.

A sketch of the built model is given in Figure 2. Table 1 provides the basic details of the FE model. A full three-dimensional model was chosen because the same model will be used in future studies for cases with stress variations in the thickness direction. All calculations were performed assuming linear elastic material properties corresponding to typical aluminium alloys. The applied boundary conditions are sketched in Fig. 2b. The displacement u for the node in the mid-thickness of the specimen at the centre of the lower fixture hole was constrained rigidly. For the corresponding node in the centre position of the upper fixture, u_x and u_z were blocked, allowing movement only in the y direction. To this single node, the external load F was applied. To prevent rigid body motion, the displacement in the z direction was blocked for a third

Table 1: Details of the built FE model.

Property	Description
Model dimensions	125 mm x 120 mm x 5 mm
Element edge lengths	1.25 mm x 1.25 mm x 1.25 mm
Number of elements	$\approx$ 38 000
Type of elements	C3D8 (ABAQUS)
Number of Nodes	$\approx$ 50 000
Degrees of freedom	$\approx$ 150 000
Young's Modulus E	73 000 MPa
Poisson's ratio ν	0.33
Contact (when used)	hard contact

node lying on the symmetry plane of the specimen on the right boundary of the model, as marked in Fig. 2b.

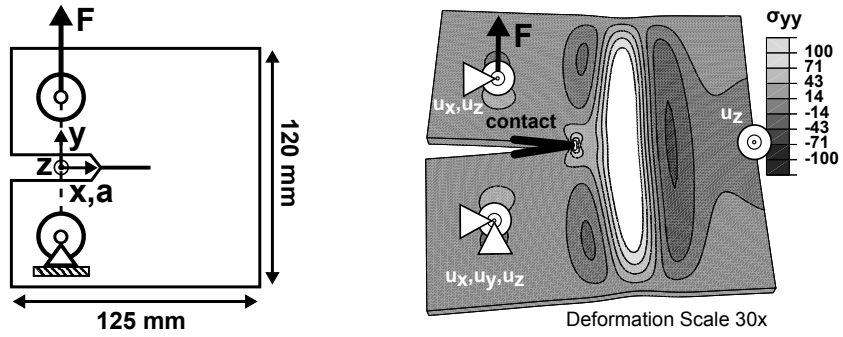

(a) (b)

Figure 2: (a) Sketch of the C(T)100 specimen geometry with the orientation definitions used and (b) the calculated longitudinal stress σ_{yy} for a model containing a crack and the mapped residual stresses under an applied load. In addition, the applied boundary conditions are sketched.

The stress profile shown in Fig. 1 was mapped on the model as the stress component σ_{yy} acting perpendicular to the crack growth direction and with no gradient through the thickness (plane stress condition). The non-equilibrium state that results from this procedure was allowed to reach the mechanical equilibrium in a first simulation step before the extraction of K_{tot}.

For the extraction of K_{tot} for different crack lengths the model was incrementally cut open along the specified crack path, allowing the crack faces behind the crack tip to move independently, including opening and overlapping.

For the simulations without contact definition on the crack faces, the resulting model was used without further changes. For the simulations including contact, a hard contact condition was added between starter notch tip and crack tip to prevent an overlapping of the crack faces in this area. Since in real

specimens the starter notch is that wide that no contact can occur, no contact condition was added to the starter notch faces.

2.3. Calculation of K_{tot}

Using the Modified Virtual Crack Closure Technique (MVCCT), which is described in more detail for example in [13, 18], the total energy release rate G_{tot} was extracted for each crack length using the specimen thickness t, the cutting forces F_{cut} of the Crack Tip Nodes (CTN) and the displacements u of the nodes located on the crack faces at a distance Δa behind the crack tip in Eq. (3). The total stress intensity factor K_{tot} can be calculated using G_{tot} in Eq. (4), where E is the Young's Modulus and ν is the Poisson's ratio. Equation (4) is based on the plane stress condition [13] and was extended by a distinction of cases to assure that crack face overlapping resulted in negative values of K_{tot}.

$$G_{\mathrm{tot}} = \frac{\sum_{CTN} F_{\mathrm{cut}} \cdot u}{t \cdot \Delta a} \tag{3}$$

$$K_{\mathrm{tot}} = \begin{cases} -1 \cdot \sqrt{\mid G_{\mathrm{tot}} \mid \cdot E} & \text{, if } F_{\mathrm{cut}} < 0 \text{ and } u < 0 \\ 1 \cdot \sqrt{G_{\mathrm{tot}} \cdot E} & \text{, if } F_{\mathrm{cut}} \geq 0 \text{ and } u \geq 0 \\ 0 & \text{, else} \end{cases} \tag{4}$$

A comparison of the numerically calculated stress intensity factor K_{tot}, for the reference model without residual stresses ("No RS"), and the handbook solution given in ASTM E647 ("Formula ASTM E647") [21], for the case of a constant applied load of $F = 4.10$ kN and 20 mm $< a <$ 80 mm gave a relative mean deviation of 3 % and a maximum deviation of 8 %.

To judge on the influence of the meshing on the calculated K_{tot}, a second model with a refined element edge length of 0.25 mm along the crack path was prepared and K_{tot} was also extracted for this model. A comparison to the original results from the model with the element edge length of 1.25 mm showed a relative mean deviation of 0.3 % and a maximum deviation of 1 %. Hence, it can be concluded that using the element edge length of 1.25 mm is sufficient for reaching the desired accuracy of K_{tot}.

2.4. Calculation of ΔK_{tot}, R_{tot}

The conditions at the crack tip under fatigue loading can be described using the total stress intensity factor range ΔK_{tot} and stress intensity factor ratio R_{tot} caused by the cyclic loading. In the absence of negative K_{tot}, these two quantities can be defined as given in Eq. (5) and Eq. (6). Here, F_{max} represents the maximum and F_{min} the minimum applied load of a load cycle.

$$\Delta K_{\mathrm{tot}} = K_{\mathrm{tot}}(F_{\mathrm{max}}) - K_{\mathrm{tot}}(F_{\mathrm{min}}) \tag{5}$$

$$R_{\mathrm{tot}} = \frac{K_{\mathrm{tot}}(F_{\mathrm{min}})}{K_{\mathrm{tot}}(F_{\mathrm{max}})} \tag{6}$$

As discussed before, if crack face overlapping is allowed, negative K_{tot} can also be observed in the calculations. The simplest way to resolve this scenario [6, 7] is a simple extension of the definitions of Eq. (5) and Eq. (6), as proposed by Parker [7] implying that $K_{\mathrm{tot}}(F_{\mathrm{max}})$ is always positive:

$$\Delta K_{\mathrm{tot}} = \begin{cases} K_{\mathrm{tot}}(F_{\mathrm{max}}) & \text{, if } K_{\mathrm{tot}}(F_{\mathrm{min}}) \leq 0 \\ K_{\mathrm{tot}}(F_{\mathrm{max}}) - K_{\mathrm{tot}}(F_{\mathrm{min}}) & \text{, if } K_{\mathrm{tot}}(F_{\mathrm{min}}) > 0 \end{cases} \tag{7}$$

$$R_{\mathrm{tot}} = \begin{cases} 0 & \text{, if } K_{\mathrm{tot}}(F_{\mathrm{min}}) \leq 0 \\ \frac{K_{\mathrm{tot}}(F_{\mathrm{min}})}{K_{\mathrm{tot}}(F_{\mathrm{max}})} & \text{, if } K_{\mathrm{tot}}(F_{\mathrm{min}}) > 0 \end{cases} \tag{8}$$

The basic idea underlying Eq. (7) is that only that part of the fatigue cycle can contribute to the crack growth in which the crack faces are opened behind the crack tip. This corresponds to the situation in which the crack tip experiences a "tensile mode I" condition [10]. Following the same argument, R_{tot} is also defined to be zero in Eq. (8) as long as the crack faces overlap under the minimum applied load. These definitions are the most simple and commonly used approach to deal with the occurrence of negative K_{tot} during the calculations [6, 7, 10]. Hence, they are also used in this work for the calculations without contact definition on the crack faces.

2.5. Prediction of $\mathrm{d}a/\mathrm{d}N$

Since the introduction of residual stresses can lead to changes of K_{tot} and R_{tot}, an empirical crack growth law is needed for the prediction of the fatigue crack propagation rate $\mathrm{d}a/\mathrm{d}N$, which is also sensitive to both K_{tot} and R_{tot}. The Walker equation [22] given in Eq. (9) is the simplest empirical crack growth law to fulfil this demand [13]. Thus, it will be used in the later sections of this work with the material parameters $C = 4.8^{-11}$ m/cycle, $n = 3.2$ and $m = 0.6937$ of the aircraft aluminium alloy A2024-T351 taken from [13].

$$\frac{\mathrm{d}a}{\mathrm{d}N} = C \left[\Delta K_{\mathrm{tot}} \left[1 - R_{\mathrm{tot}} \right]^{m-1} \right]^{n} \tag{9}$$

2.6. Prediction of the crack length as a function of the loading cycles $a(N)$

The number of loading cycles N until reaching a specific crack length a can be obtained by the integration of the inverse of the predicted crack growth rates, which, in this case, is the Walker equation given in Eq. (9).

$$\int_0^N \mathrm{d}N = \int_{a_0}^{a} \left(C \left[\Delta K_{\mathrm{tot}} \left[1 - R_{\mathrm{tot}} \right]^{m-1} \right]^{n} \right)^{-1} \mathrm{d}a \tag{10}$$

The right-hand side of Eq. (10) can be evaluated by numerical integration using the corresponding calculated ΔK_{tot} and R_{tot} as supporting points to obtain the function $N(a)$. Under the assumption that crack growth rates are always larger than zero, the inverse function exists and provides the desired crack length as a function of the number of loading cycles $a(N) = N(a)^{-1}$.

3. Results and Discussion

3.1. Simulation Cases

FE simulations were performed with a constant $\Delta K_{\mathrm{appl}} = 20\ \mathrm{MPa}\sqrt{\mathrm{m}}$ and a constant $R_{\mathrm{appl}} = 0$. Thus, the minimum applied external load during the load cycle was set to zero. The needed maximum applied load $F_{\mathrm{appl}}(a)$ to reach constant $K_{\mathrm{appl}}(F_{\mathrm{appl}}) = 20\ \mathrm{MPa}\sqrt{\mathrm{m}}$ was recalculated for each crack length. The numerical simulations were performed for crack lengths $20\ \mathrm{mm} \leq a \leq 80\ \mathrm{mm}$ and the following cases:

- No residual stresses ("No RS")
- Residual stresses without contact definition on the crack faces ("RS & No Contact")
- Residual stresses with contact definition on the crack faces ("RS & Contact")

The crack growth increment da lying between two calculation steps was equal to an element edge length along the crack path of 1.25 mm.

3.2. Calculation of K_{tot}

Figure 3 shows the initial residual stress profile (upper graph) and the resulting calculated K_{tot} (middle graph). The evolution of the normalised total strain energy (lower graph) for the two simulation cases including residual stresses is needed for the discussion given later in section 3.3.

For the case "No RS" a constant $K_{\mathrm{tot}}(F_{\mathrm{appl}}) = 20\ \mathrm{MPa}\sqrt{\mathrm{m}}$ and a constant $K_{\mathrm{tot}}(0\ \mathrm{kN}) = 0\ \mathrm{MPa}\sqrt{\mathrm{m}}$ is calculated, indicating, that the recalculation of the $F_{\mathrm{appl}}(a)$ was correct.

For the cases "RS & No Contact" and "RS & Contact" the calculation of $K_{\mathrm{tot}}(F_{\mathrm{appl}})$ leads to identical results, indicating that under the maximum applied load, the crack faces are completely open for any crack length a. Hence, there is no impact of the contact definition. The visible modulation of $K_{\mathrm{tot}}(F_{\mathrm{appl}})$ is caused by the residual stress field. As shown in Fig. 3, compressive residual stresses lead to a decrease of $K_{\mathrm{tot}}(F_{\mathrm{appl}})$ and tensile residual stresses increase $K_{\mathrm{tot}}(F_{\mathrm{appl}})$. Since the stress intensity factor is not governed by the stress state at the crack tip alone, but by the whole stress field acting on the crack faces, the modulation of $K_{\mathrm{tot}}(F_{\mathrm{appl}})$ follows the residual stress profile with a certain delay.

In the absence of a contact definition ("RS & No Contact"), the curve of $K_{\mathrm{tot}}(0\ \mathrm{kN})$ is simply shifted down by $20\ \mathrm{MPa}\sqrt{\mathrm{m}}$ with respect to the calculated $K_{\mathrm{tot}}(F_{\mathrm{appl}})$, proofing that for this linear case the superposition principle is valid.

The definition of contact on the crack faces ("RS & Contact") changes the behaviour essentially. While the crack tip is subjected to compressive residual stresses, the total stress intensity $K_{\mathrm{tot}}(0\ \mathrm{kN})$ is zero, showing that the crack faces at the crack tip are in contact. However, right after the crack tip enters the area of tensile residual stress, a positive stress intensity is observed. In

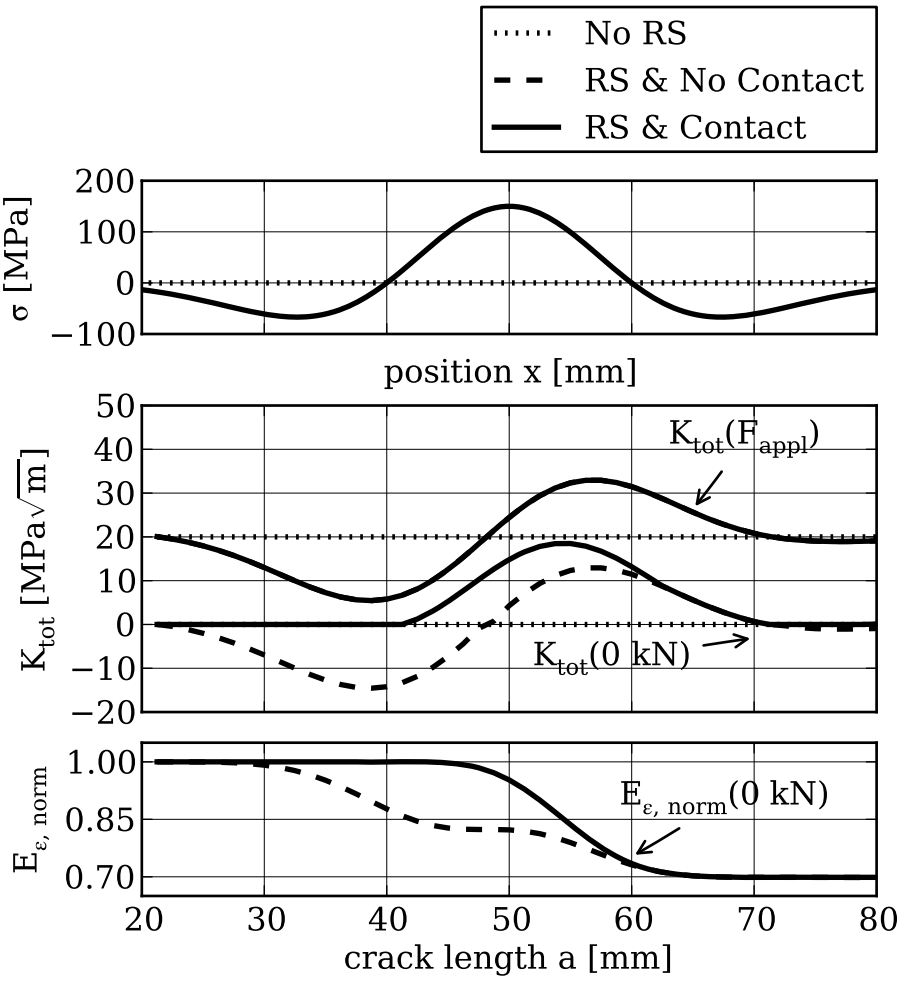

Figure 3: Mapped initial residual stress profiles (top), calculated total stress intensity factor K_{tot} (middle) and the normalised stored strain energy without applied load $E_{\epsilon,\mathrm{norm}}(0\ \mathrm{kN})$ (bottom).

the following, $K_{\mathrm{tot}}(0\ \mathrm{kN})$ increases quickly compared to the simulation without contact and reaches much higher values. The delay with which the stress profile is followed is substantially smaller.

Passing the second transition from tensile to compressive residual stresses at $a = 60$ mm, no substantial difference for $K_{\mathrm{tot}}(0\ \mathrm{kN})$ can be found when comparing the predictions with and without contact.

3.3. Energy based discussion of the observed differences with and without contact

The discussed differences of the extracted $K_{\mathrm{tot}}(0\ \mathrm{kN})$ for the simulation cases "RS & No Contact" and "RS & Contact" can be explained by comparing the evolution of the stored strain energy normalised to its initial value without crack and without applied load $E_{\epsilon,\mathrm{norm}}(0\ \mathrm{kN})$ shown in Fig. 3 (bottom).

For the model without contact definition, the strain energy is minimised by the overlap of the crack faces, leading to negative values of $K_{\mathrm{tot}}(0\ \mathrm{kN})$. Even when the crack tip is already subjected to tensile residual stresses, the crack faces remain overlapped because this state is still linked to the minimum of the strain energy.

In the simulation with contact only an opening of the crack faces but no overlapping of them is allowed. While the crack faces are completely subjected to compressive residual stresses the crack remains closed, resulting in a $K_{\mathrm{tot}}(0\ \mathrm{kN})$ of zero and a constant strain energy. However, as soon as the crack tip enters the area of tensile residual stresses, the crack faces can open partially at the crack tip and the strain energy drops.

In Fig. 4, this different behaviour in the crack opening is demonstrated for a crack of length $a = 47.5$ mm and without applied load. At this crack length, the crack tip already has passed the transition from compressive to tensile residual stresses at $a = 40$ mm. For clarity only the profile of the upper crack faces is shown. For the case "RS & No Contact", the crack faces completely overlap as indicated by the negative values of u. For the case "RS & Contact", a partial contact of the crack faces can be found in the area subjected to compressive residual stresses ($u = 0$ mm), while a partial opening can be found for the area subjected to tensile residual stresses ($u > 0$ mm).

As shown in Fig. 5, for $a \geq 63.75$ mm, the crack faces are completely open along the whole crack length even without an applied load. Therefore the contact definition on the crack faces does no longer influence the simulation result, and the calculated $K_{\mathrm{tot}}(0\ \mathrm{kN})$ with and without contact are identical.

3.4. Calculation of ΔK_{tot}, R_{tot} and $\mathrm{d}a/\mathrm{d}N$

Figure 6 shows ΔK_{tot}, R_{tot} and $\mathrm{d}a/\mathrm{d}N$ calculated on the basis of the stress intensity factor data given in Fig. 3, using Eq. (7), Eq. (8) and Eq. (9). The reference case without residual stresses shows the desired constant $\Delta K_{\mathrm{tot}} = \Delta K_{\mathrm{appl}} = 20\ \mathrm{MPa}\sqrt{\mathrm{m}}$ and $R_{\mathrm{tot}} = R_{\mathrm{appl}} = 0$. Accordingly, for this case, the calculated crack growth rate using the AA2024-T351 material data taken from [13] is constant as well.

Because the negative $K_{\mathrm{tot}}(0\ \mathrm{kN})$ are set to zero during the calculation of ΔK_{tot}, as defined in Eq. (7) and Eq. (8), the calculations with and without

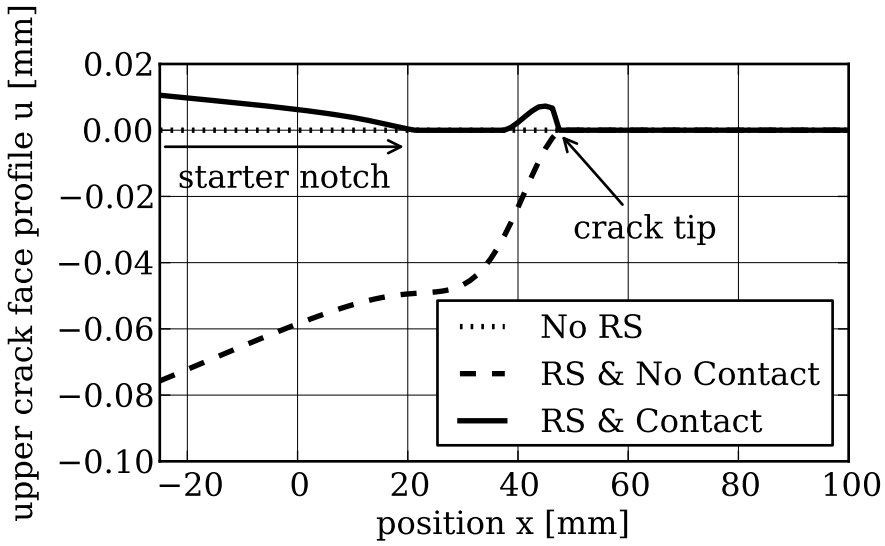

Figure 4: Displacement u of the upper crack faces after the introduction of a crack with length $a = 47.5$ mm without applied load. The lower crack faces moved exactly symmetrically (not shown). Negative values indicate overlapping.

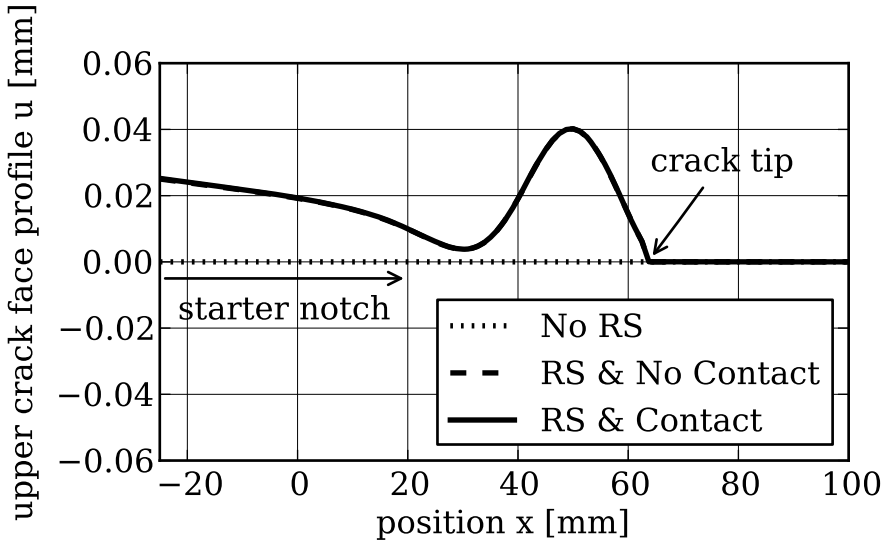

Figure 5: Displacement u of the upper crack faces after the introduction of a crack with length $a = 63.75$ mm without applied load. The lower crack faces moved exactly symmetrically (not shown). Negative values indicate overlapping.

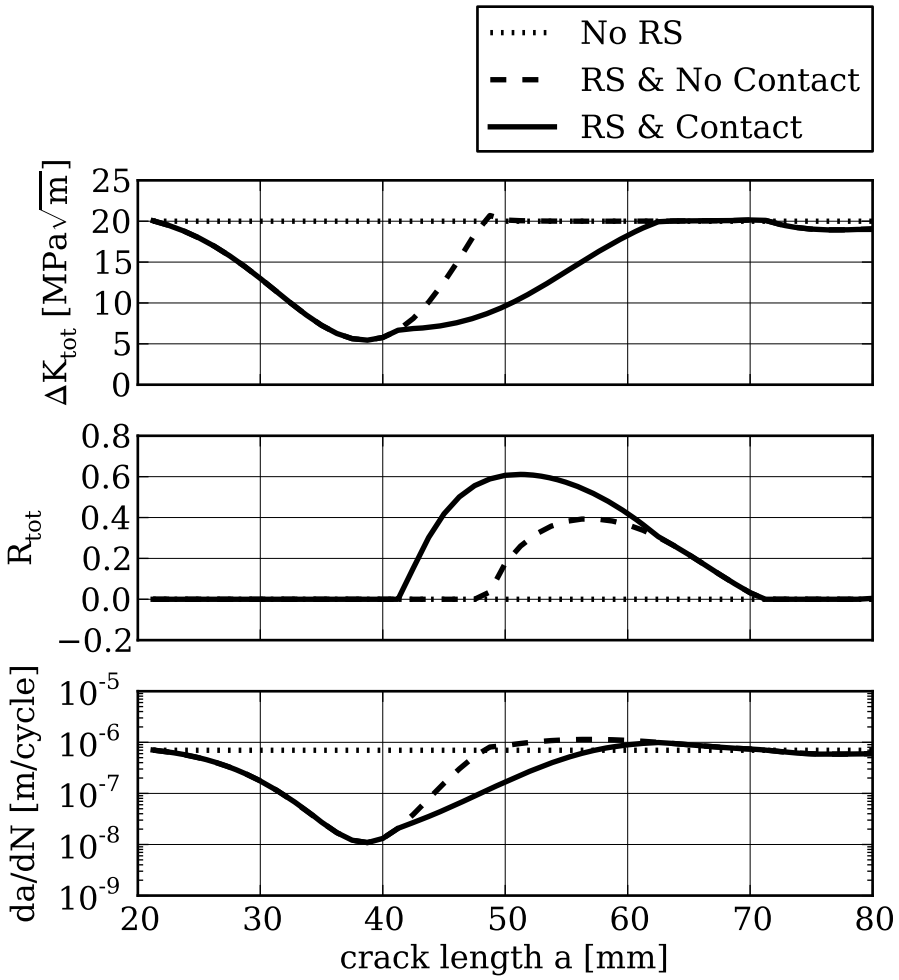

Figure 6: Calculated total stress intensity factor range ΔK_{tot} (top), total stress intensity factor ratio R_{tot} (middle) and fatigue crack propagation rate $\mathrm{d}a/\mathrm{d}N$ (bottom).

contact lead to the same results for 20 mm $< a <$ 40 mm and 62.5 mm $< a <$ 80 mm.

However, for 41.25 mm $\leq a \leq$ 62.5 mm, the predictions differ substantially. For the case "RS & No Contact", the calculated ΔK_{tot}, shown in Fig. 6, follow simply the modulation of $K_{\mathrm{tot}}(F_{\mathrm{appl}})$ (Fig. 3). Because the profiles of the curves for $K_{\mathrm{tot}}(0\ \mathrm{kN})$ and $K_{\mathrm{tot}}(F_{\mathrm{appl}})$ are identical, ΔK_{tot} reaches a constant value of 20 MPa$\sqrt{\mathrm{m}}$ as soon as $K_{\mathrm{tot}}(0\ \mathrm{kN})$ becomes positive. From this point onwards, R_{tot} becomes positive and follows the modulation of $K_{\mathrm{tot}}(0\ \mathrm{kN})$ and $K_{\mathrm{tot}}(F_{\mathrm{appl}})$. Thus, until $K_{\mathrm{tot}}(0\ \mathrm{kN})$ turns positive, the crack growth is retarded in comparison to the case "No RS". Afterwards, the predicted crack growth rate is slightly above the reference case without residual stresses because the increase of R_{tot} leads to an acceleration of the predicted crack growth.

For the case "RS & Contact" the rapid increase of $K_{\mathrm{tot}}(0\ \mathrm{kN})$ to high positive values directly after the crack tip entered the area of tensile residual stresses ($a \geq$ 41.25 mm) leads to a significant decrease of ΔK_{tot} and an increase of R_{tot} at the same time. While a decrease of ΔK_{tot} retards crack growth, an increase of R_{tot} accelerates it. However, for the case presented with the material constants of the aircraft aluminium alloy AA2024-T351, the calculations with a contact definition on the crack faces lead to an equal or smaller predicted crack growth rate for any crack length compared to the calculations without contact.

3.5. Prediction of the crack length as a function of the loading cycles $a(N)$

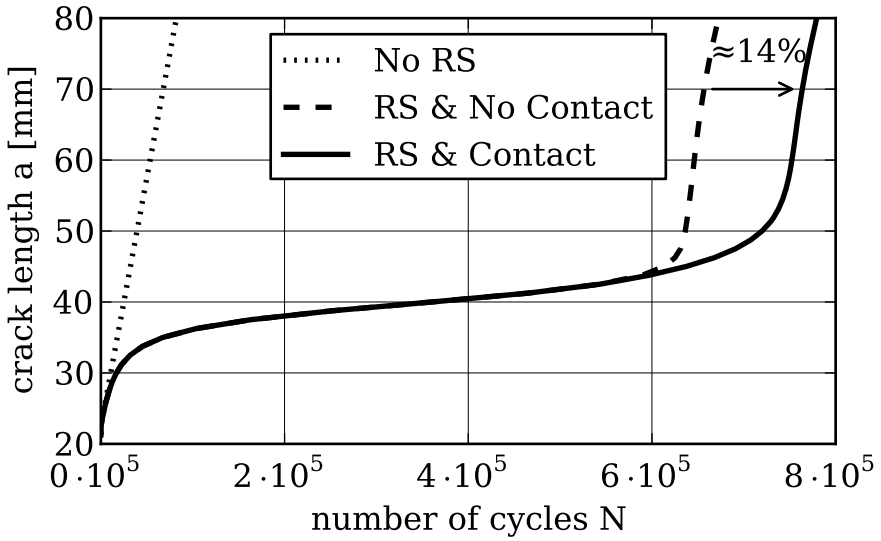

Figure 7: Calculated crack length as a function of the load cycles $a(N)$ based on the predicted fatigue crack growth rates calculated using the Walker Equation Eq. (9) with AA2024 material constants.

Figure 7 shows the results of the numerical integration of the fatigue crack growth rates presented in Fig. 6. To reach a final crack length of $a = 80$ mm, the predicted number of loading cycles for the calculations with contact is approximately 14% higher than for the calculations without contact.

3.6. Generalisation to arbitrary materials and stress profiles

In the following, a generalisation of the observed effect, that the calculations with a contact definition on the crack faces lead to an equal or smaller predicted crack growth rate for any crack length compared to the predictions without contact, is given.

Using the definitions in Eq. (8) and Eq. (7), it is possible to replace the functional dependence of $\mathrm{d}a/\mathrm{d}N$ on R_{tot} by a functional dependence on $K_{\mathrm{tot}}(F_{\mathrm{appl}})$ in the form of Eq. (11).

$$\begin{aligned}
\frac{\mathrm{d}a}{\mathrm{d}N} &= C\left[\Delta K_{\mathrm{tot}}\left[1-R_{\mathrm{tot}}\right]^{m-1}\right]^{n} \\
&= C\left[\left[K_{\mathrm{tot}}(F_{\mathrm{appl}})-K_{\mathrm{tot}}(0\ \mathrm{kN})\right]\left[1-\frac{K_{\mathrm{tot}}(0\ \mathrm{kN})}{K_{\mathrm{tot}}(F_{\mathrm{appl}})}\right]^{m-1}\right]^{n} \\
&= C\left[\left[\Delta K_{\mathrm{tot}}\right]^{m}\left[K_{\mathrm{tot}}(F_{\mathrm{appl}})\right]^{1-m}\right]^{n} \qquad (11)
\end{aligned}$$

As previously shown in Fig. 3, $K_{\mathrm{tot}}(F_{\mathrm{appl}})$ is not influenced by the introduction of contact as long as the crack is completely open, for any crack length under the maximum applied load F_{appl}. Additionally, the exponent m in the Walker equation only varies between zero and one. Under these conditions, smaller ΔK_{tot} always lead to smaller $\mathrm{d}a/\mathrm{d}N$ independent of R_{tot}. As shown in Fig. 6, for the presented case the calculations with contact showed equal or smaller ΔK_{tot} for any crack length compared to the calculations without contact. Thus, also the predicted $\mathrm{d}a/\mathrm{d}N$ using contact must be equal or smaller than the $\mathrm{d}a/\mathrm{d}N$ predicted without contact, independent of the material constants used in Eq. (11).

If no external load is applied and a contact condition is present, the internal energy can only be released by local opening of the crack in an area of tensile stresses. For the case where no contact is defined, the internal energy is automatically minimised by an overlapping of the crack faces in the areas of compressive residual stresses. Thus, independent of the exact shape and the amplitude of the residual stress distribution, it can be stated that when the crack tip reaches a transition from compressive to tensile residual stresses, a simulation using contact on the crack faces must show an equal or a higher internal energy compared to one without contact definition. Thus, also the driving force for energy release is in any case equal or higher for the model including contact. Since the stress intensity factor can be directly linked to the energy release rate as given in Eq. (4), this should always lead to higher $K_{\mathrm{tot}}(0\ \mathrm{kN})$. If contact is defined and the crack is completely open under the maximum applied load,

this results in smaller ΔK_{tot} and $\mathrm{d}a/\mathrm{d}N$, independent of the exact shape of the stress profile.

Both aspects together give a clear indication that calculations using a contact definition on the crack faces always lead to equal or smaller predicted $\mathrm{d}a/\mathrm{d}N$ compared to calculations without contact, independent from both the actual material properties used and the exact shape and amplitude of the stress profile.

4. Conclusion

As an representative example, the fatigue crack growth in an aluminium AA2024 C(T)100 specimen, containing an assumed welding like residual stress field, was predicted. Differences in the prediction results were discussed, comparing the commonly used methodology that neglects contact of the crack faces and the one using a contact definition on the crack faces.

The calculated results for K_{tot} showed significant differences for the simulations with and without contact, especially when the crack tip moved through the transition region from compressive to tensile residual stresses. These differences could be explained by the effect of the contact condition on the local opening behaviour of the crack faces near the crack tip.

For the discussed representative example, the predicted number of load cycles to reach a final crack length of 80 mm was approximately 14% higher for the calculations with contact than for the calculations without contact.

There is strong indication that calculations not including contact always lead to the same or shorter predicted total lifetimes compared to ones using contact. However, the significance of the effect strongly depends on the actual material properties, the exact shape of the residual stress profile and the position of the stress profile relative to the crack.

Compared to the commonly used methodology that neglects contact, the use of a contact definition on the crack faces for the predictions can be seen as an extension, that helps to describes the real experimental conditions physically sound for specific cases. Hence, accounting for contact in the predictions can help to improve the prediction quality.

These findings motivated to employ the presented modelling approach with a hard contact definition on the crack faces as part of a quantitative prediction methodology for the fatigue crack growth in C(T)100 specimens containing laser heating induced residual stresses. The development of the prediction methodology also including process simulation and a stepwise validation of the predictions on basis of experimental results is reported in [23, 24].

Acknowledgements

The authors wish to thank Dr. Waman Vishwanath Vaidya of Helmholtz-Zentrum Geesthacht, Germany, and Dr. Xiang Zhang of Cranfield University, UK, for valuable discussions.

References

[1] Schmidt HJ. Damage tolerance technology for current and future aircraft structures. In: Donne CD, editor. Proceedings of the 23rd ICAF Symposium of the international Committee on Aeronautical Fatigue; vol. 1. 2005, p. 1–41.

[2] Kocik R, Vugrin T, Seefeld T. Laserstrahlschweissen im Flugzeugbau: Stand und künftige Anwendungen. In: Strahltechnik; vol. 28. BIAS; 2006, p. 15–26.

[3] Staron P, Vaidya WV, Koçak M, Homeyer J, Hackius J. Residual stresses in laser beam welded butt joints of the airframe aluminium alloy AA6056. Materials Science Forum 2006;524–525:413–418.

[4] Machold W, Staron P, Bayraktar F, Riekehr S, Koçak M, Schreyer A. Influence of the welding sequence on residual stresses in laser welded T-joints of an airframe aluminium alloy. Materials Science Forum 2008;571–572:375–380.

[5] Zhang X, Irving P, Edwards L, Fitzpatrick M, Sinclair I, Lin J, et al. The influence of residual stress on design and damage tolerance of welded aircraft structures. In: Donne CD, editor. Proceedings of the 23rd ICAF Symposium of the International Committee on Aeronautical Fatigue; vol. 1. 2005, p. 265–281.

[6] Irving P, Ma YE, Zhang X, Servetti G, Williams S, Moore G, et al. Control of crack growth rates and crack trajectories for enhanced fail safety and damage tolerance in welded structures. In: Procceding of the 25th ICAF Symposium. 2009, p. 387–405.

[7] Parker A. Stress Intensity Factors, Crack Profiles and Fatigue Crack Growth Rates in Residual Stress Fields. In: Throop JF, Reemsnyder HS, editors. Residual Stress Effects in Fatigue; vol. ASTM STP 776. ASTM; 1982, p. 13–31. doi:10.1520/STP776-EB.

[8] Lee YB, Chung CS, Park YK, Kim HK. Effects of redistributing residual stress on the fatigue behavior of SS330 weldment. International Journal of Fatigue 1998;20:565–573.

[9] Mahmoud HN, Dexter RJ. Propagation rate of large cracks in stiffened panels under tension loading. Marine Structures 2005;18(3):265–288. doi: 10.1016/j.marstruc.2005.09.001.

[10] Edwards L. Influence of residual stress redistribution on fatigue crack growth and damage tolerant design. Materials Science Forum 2006;524-525:77–82.

[11] Labeas G, Diamantakos I. Numerical investigation of through crack behaviour under welding residual stresses. Engineering Fracture Mechanics 2009;76(11):1691–1702. doi:10.1016/j.engfracmech.2009.03.006.

[12] Liljedahl C, Brouard J, Zanellato O, Lin J, Tan M, Ganguly S, et al. Weld residual stress effects on fatigue crack growth behaviour of aluminium alloy 2024-T351. International Journal of Fatigue 2009;31(6):1081–1088. doi:10.1016/j.ijfatigue.2008.05.008.

[13] Servetti G, Zhang X. Predicting fatigue crack growth rate in a welded butt joint: The role of effective R ratio in accounting for residual stress effect. Engineering Fracture Mechanics 2009;76(11):1589–1602. doi:10.1016/j.engfracmech.2009.02.015.

[14] Bao R, Zhang X, Yahaya NA. Evaluating stress intensity factors due to weld residual stresses by the weight function and finite element methods. Engineering Fracture Mechanics 2010;77(13):2550–2566. doi:10.1016/j.engfracmech.2010.06.002.

[15] Beghini M, Bertini L. Fatigue crack propagation through residual stress fields with closure phenomena. Engineering Fracture Mechanics 1990;36(3):379–387. doi:10.1016/0013-7944(90)90285-O.

[16] Beghini M, Bertini L, Vitale E. Fatigue crack growth in residual stress fields: Experimental results and modelling. Fatigue & Fracture of Engineering Materials & Structures 1994;17:1433–1444. doi:10.1111/j.1460-2695.1994.tb00786.x.

[17] Terada H. Stress intensity factor analysis and fatigue behavior of a crack in the residual stress field of welding. Journal of ASTM International 2005;2(5). doi:10.1520/JAI12558.

[18] Richter-Trummer V, Tavares S, Moreira P, de Figueiredo M, de Castro P. Residual stress measurement using the contour and the sectioning methods in a MIG weld : Effects on the stress intensity factor. Ciência e Tecnologia dos Materiais 2008;20:115–119.

[19] Anifantis NK. Crack surface interference: a finite element analysis. Engineering Fracture Mechanics 2001;68(12):1403–1415. doi:10.1016/S0013-7944(01)00028-5.

[20] Tada H, Paris P, Irwin G. The Stress Analysis of Cracks Handbook. Professional Engineering Publishing; 3 ed.; 2000.

[21] ASTM E647-05 Standard Test Method for Measurement of Fatigue Crack Growth Rates. 2005.

[22] Walker K. The effect of stress ratio during crack propagation and fatigue for 2024-T3 and 7075-T6. In: Effects of enviroment and complex load history on fatigue life; vol. STP 462. ASTM; 1970, p. 1–14.

[23] Schnubel D, Horstmann M, Ventzke V, Riekehr S, Staron P, Fischer T, et al. Retardation of fatigue crack growth in aircraft aluminium alloys via laser heating - Experimental proof of concept. Submitted for publication 2011.

[24] Schnubel D, Huber N. Retardation of fatigue crack growth in aircraft aluminium alloys via laser heating - Numerical prediction of fatigue crack growth. Submitted for publication 2011.